JOURNAL OF CATALYSIS **169,** 250–262 (1997)
ARTICLE NO. CA971635

Kinetic Study of the Carbon Filament Formation by Methane Cracking on a Nickel Catalyst

J.-W. Snoeck,*[,1] G. F. Froment,*[,2] and M. Fowles†

*Laboratorium voor Petrochemische Techniek, Universiteit Gent, Krijgslaan 281, B-9000 Gent, Belgium; and †ICI Katalco, P.O. Box 1, Billingham, Cleveland TS23 1LB, England

Received May 28, 1996; revised January 29, 1997; accepted February 3, 1997

A rigorous kinetic model for the formation of filamentous carbon on a nickel catalyst by methane cracking is derived. The experimental study was performed in an electrobalance unit. The temperature ranged from 773 to 823 K and the partial pressure of methane ranged from 1.5 to 10 bar. The mode of experimentation ensured that the rate of growth of the carbon filaments was always based upon the same number of filaments. A kinetic model is selected in which the abstraction of the first hydrogen atom from molecularly adsorbed methane is the rate-determining step. Based on the results of the parameter estimation, an energy diagram for the methane cracking is constructed.

INTRODUCTION

Because of its importance in catalyst deactivation and fouling of reactor tubes the deposition of carbon deposits on metal surfaces by the decomposition of carbon containing gases has been studied for many years (1–3). Natural gas, which consists mainly of methane, is used as a feedstock in the steam reforming of hydrocarbons for the production of synthesis gas. A major problem in this process is the formation of filamentous carbon, which is able to desintegrate the catalyst support structure, leading to blockage of the reactor (3).

The results for the methane cracking reported here are part of a study which aims at the development of a global model describing the formation and the gasification of carbon from a steam reforming mixture. Studies of the Boudouard reaction, the gasification by carbon dioxide, hydrogen, and steam, and the construction of the global model were also part of this study.

The interaction of methane with nickel surfaces has been studied using molecular beam techniques combined with HREELS (high-resolution electron energy loss spectroscopy) (5–9) and by "high"-pressure studies ($p = 1$ Torr) using AES (Auger electron spectroscopy) to follow the rate of carbon buildup (10–13). A combination of the molecular beam technique with HREELS showed that the chemisorption of methane is dissociative and that the nascent product of the dissociative chemisorption is an adsorbed methyl group that gradually dehydrogenates on the surface at higher temperatures (5, 6). The barrier to dissociative chemisorption of methane arises from the energy required to deform the methane molecule, to an extent that the attractive interactions between C and the Ni surface become sufficiently large to result in the formation of the Ni–C bond (7, 8). The studies by AES also indicate that methane adsorbs dissociatively on Ni through a direct process, i.e., not involving a precursor state (12, 13).

Kinetic studies of methane cracking in a microbalance reactor were recently reported (14–16). Alstrup *et al.* (14, 15) performed a kinetic study of the methane cracking at atmospheric pressure and proposed a mechanism with a stepwise dehydrogenation of the surface species after a direct dissociative adsorption of methane. Both the dissociative chemisorption step and the dehydrogenation of the adsorbed methyl group would be rate determining. Scrutiny of their results at different temperatures indicates that it is more probable that the dissociative adsorption step is rate determining (15).

In this paper, the results of a kinetic study of the methane cracking at high pressure in an electrobalance reactor are presented. The derivation of the kinetic models, based on a detailed description of the mechanism of carbon filament formation, is explained. The finally selected model is extensively compared with literature data.

EXPERIMENTAL

Materials

The catalyst used in this study was the ICI 46-9P steam-reforming catalyst and was described in a previous paper (17). The gases with a purity >99.95% were purchased from L'Air Liquide.

Equipment and Procedure

The experimental installation was described in a previous paper (17). Only a few comments will be given here.

[1] Present address: BASF Antwerpen, Scheldelaan 600, B-2040 Antwerpen, Belgium.

[2] To whom correspondence should be addressed.

0021-9517/97 $25.00

The bypass of the catalyst basket by an important part of the feed necessitates differential operation, to obtain the correct relationship between the experimentally observed rate and the feed composition. Differential operation is reached when the conversion over the catalyst bed is so small that the change in composition over the catalyst bed does not influence the rate of carbon formation. It is limited to the linear part of the conversion versus space time curve. Differential operation was checked, for a number of experiments. For the most severe conditions, the conversion of methane, based on the feed flow rate through the catalyst bed in the basket, was below 1.5%.

A check for external and internal diffusional limitations was performed using the guidelines described in Froment and Bischoff (18). For the range of experimental conditions of this study there were no internal or external gradients of concentration or temperature.

Because the thermodynamic properties of the carbon deposit are not known, the coking threshold, i.e., the conditions for which the rate of carbon formation equals the rate of gasification was determined experimentally. This involved a gradual increase of the partial pressure of hydrogen, while maintaining the partial pressure of methane constant, until the net rate of carbon formation became zero. From these conditions, the threshold constant for the methane cracking was calculated from $K_M^* = p_{H_2}^2 / p_{CH_4}$. These experiments were performed in the most sensitive range of the electrobalance.

Experimental Program

The experiments were performed in the temperature range 773–823 K with an amount of catalyst of around 15 mg. A feed flow rate of methane of around 2.5 mol/h was chosen, which ensured differential operation. The partial pressure of methane was varied between 1.5 and 10 bar and covering the range of partial pressures encountered in industrial steam reformers. Hydrogen was always added to the feed to model the reverse reaction, but also to enable differential operation. The presence of hydrogen in the feed leads to a smaller conversion and to a smaller relative change of the hydrogen partial pressure, so that a uniform rate of carbon formation is obtained over the whole catalyst bed. The partial pressure of hydrogen was varied between 0 and 1.65 bar. The experimental conditions here were always chosen in the region with an affinity for carbon deposition. The results of experiments performed on fresh catalysts and on "used" catalysts, on which carbon was previously deposited under standard conditions, are compared.

RESULTS

Determination of the Coking Threshold

In order to obtain information regarding the thermodynamic properties of filamentous carbon, the threshold constant for the methane cracking has to be determined experimentally for a number of temperatures (17). The coking threshold refers to those conditions for which there is no carbon deposition and gasification, i.e., for which the rates of all the consecutive steps of carbon filament formation are zero. These conditions are normally referred to as the equilibrium for the methane cracking (20–23). The name coking threshold was preferred because the diffusion of carbon through nickel cannot be considered as a normal reversible surface reaction step. This also complicates the description of a reversible model for carbon filament formation, based on the experimentally determined threshold constant, as will be illustrated further in paragraph 3.

The following expression was derived for the threshold constant for the methane cracking (17). It contains the thermodynamic properties of filamentous carbon:

$$K_M^* = \left(\frac{p_{H_2}^2}{p_{CH_4}}\right)_{r_{C,M}=0} = \exp\left(-\frac{\mu_{C_{fil}} + 2\mu_{H_2}^0 - \mu_{CH_4}^0}{RT}\right). \quad [1]$$

The threshold constant was determined for various partial pressures of methane and for various temperatures. The experimentally determined values for the threshold constant are shown in Fig. 1 as a function of the temperature and are also compared with values for the equilibrium constant for the methane cracking reaction that were calculated on the basis of thermodynamic data for graphite and nickel carbide. The following expressions are obtained for the threshold constant as a function of the temperature at different

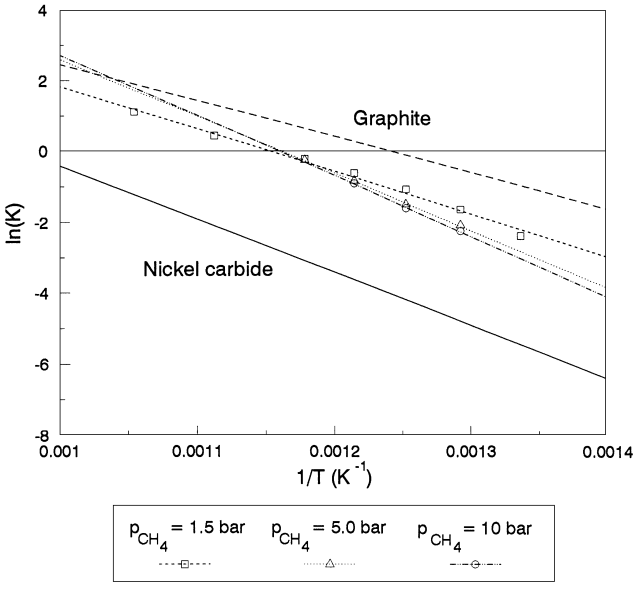

FIG. 1. lnK versus 1/*T* plot for the threshold constants for the methane cracking for different partial pressures of methane. Comparison with graphite and nickel carbide.

partial pressures of methane:

$p_{CH_4} = 1.5$ bar	$K_M^* = \exp(116.1/R) \cdot \exp(-100765/R/T)$
$p_{CH_4} = 5.0$ bar	$K_M^* = \exp(156.1/R) \cdot \exp(-134230/R/T)$
$p_{CH_4} = 10.0$ bar	$K_M^* = \exp(164.7/R) \cdot \exp(-141900/R/T)$
Graphite	$K_M^{gr} = \exp(104.8/R) \cdot \exp(-84400/R/T)$
Nickel carbide (24)	$K_M^{Ni_3C} = \exp(121.3/R) \cdot \exp(-124600/R/T)$

The standard enthalpy and entropy change for the methane cracking, derived from the expressions for the threshold constant, are clearly different from the values for graphite and nickel carbide, which is not surprising since filamentous carbon has a clearly different morphology. Furthermore, the values differ for different partial pressures of methane. It is not clear how to explain this influence. Although the exact position of the coking threshold is very difficult to determine, due to the broad range of partial pressures of hydrogen in which the rate of carbon formation varies very little, identical results were obtained after replicate experiments. Identical results were also obtained when the initial carbon formation was always performed under standard conditions, after which the normal procedure was started for the determination of the coking threshold. Therefore, the conditions during the nucleation of the carbon filaments do not explain these differences. The only similar result in the literature is the dependence of the thermodynamic properties of surface carbon on its coverage, observed by Takeuchi *et al.* (24). The determination of the coking threshold at varying partial pressures of methane implies different equilibrium carbon surface coverages, due to the competition between gas adsorption and solid segregation (17).

Experimental Results for the Methane Cracking

The influence of the partial pressure of hydrogen and methane on the rate of carbon filament formation in methane cracking at 798 K is shown in Fig. 2. Each experiment was performed on a fresh catalyst sample. The rates shown correspond to those in the linear part of the weight versus time curves, where no further nucleation of carbon filaments takes place. A strong effect of the partial pressure of hydrogen on the rate of carbon formation can be seen. This is explained by the decrease of the carbon formation affinity with increasing partial pressure of hydrogen, or by the increase of the rate of the reverse step, the gasification by hydrogen. The position of the coking threshold, determined as described in the previous paragraph, is also indicated.

At $p_{CH_4} = 1.5$ bar, a decrease of the rate of carbon formation is observed at very low partial pressures of hydrogen. At $P_{CH_4} = 1.5$ bar and $P_{H_2} = 0$ bar, the weight versus time curve reflects a fast deactivation caused by encapsulating carbon. At $P_{CH_4} = 5$ bar and $p_{CH_4} = 10.0$ bar, the curves

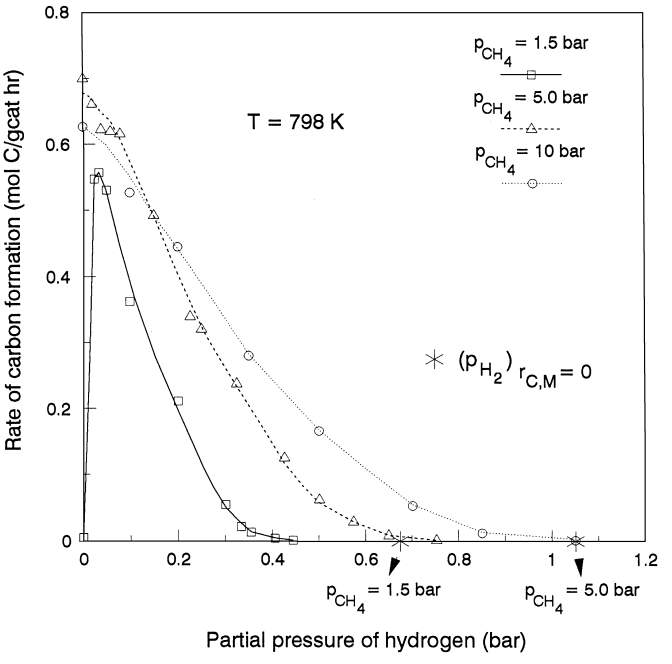

FIG. 2. Methane cracking: experimental results. Rate of carbon formation versus partial pressure of hydrogen. $T = 525°C$; $p_{CH_4} = 1.5$, 5.0, or 10.0 bar.

level off for low hydrogen partial pressures. At low partial pressure of hydrogen, the rate of carbon formation does not increase monotonously with the partial pressure of methane. This points toward the presence of a term with the partial pressure of methane in the denominator of the rate equation.

Figure 2 also shows that the rate of carbon formation becomes extremely low at partial pressures of hydrogen clearly below the coking threshold, probably because of the very difficult nucleation of carbon filaments under conditions with a low affinity for carbon formation (17). Under these conditions only a small number of growing carbon filaments is present on the catalyst sample. This biases the rates of carbon formation and also complicates the kinetic modeling. If the rate of nucleation is not explicitly included in the rate equation, all the experiments selected for the kinetic modeling should be based on the same number of growing carbon filaments. Therefore, experiments were sequentially performed on the same used catalyst sample, starting with the conditions with the highest affinity for carbon formation. The large number of carbon filaments that nucleated under these conditions is able to grow further during all the subsequent conditions with a lower affinity, so that all the rates of carbon formation are based on the same number of growing carbon filaments. In this way, reliable rates can be obtained even close to the coking threshold. The results of these sequential experiments on "used" catalyst samples at 823 K and $p_{CH_4} = 1.5$ bar are shown in Fig. 3, together with the results of the separate experiments on fresh

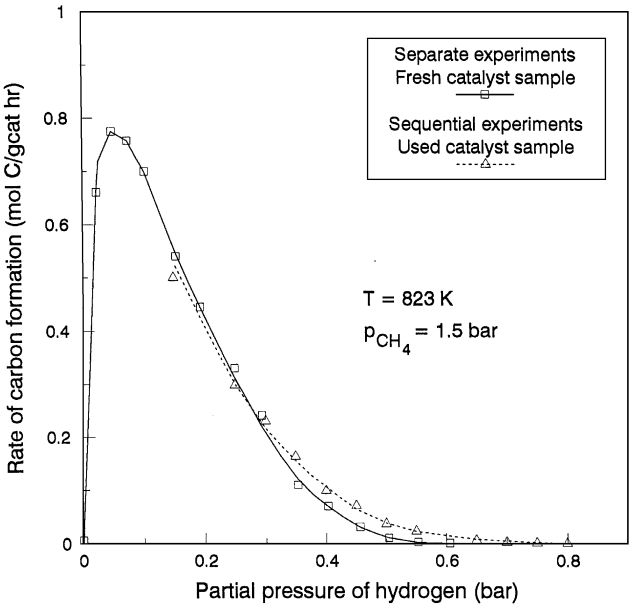

FIG. 3. Comparison of the rates of carbon formation obtained from separate experiments on fresh catalyst samples and sequential experiments on used catalyst samples. $T = 550°C$; $p_{CH_4} = 1.5$ bar.

catalyst samples. At high partial pressures of hydrogen, a difference can indeed be observed between the rates of carbon formation on fresh and used catalyst samples, due to the difficult nucleation of carbon filaments on fresh catalyst samples.

The kinetic modeling was based upon experiments on used catalysts samples. The use of the experiments on fresh catalyst samples results in model predictions for the rate of carbon formation that become negative under conditions with a clear affinity for carbon formation.

Derivation of the Kinetic Model

The kinetic modeling has to consider two aspects: the surface reactions and the carbon filament formation.

Nonreversible model description. All the possible surface reaction mechanisms for the methane cracking are shown in Fig. 4. Altogether, there are 33 possible pathways from gas-phase methane to adsorbed carbon. Methane can adsorb molecularly or dissociatively and further undergo a stepwise or saltatory dehydrogenation. Each step can be rate determining. This leads to 80 different rate equations. The primary reaction product, adsorbed carbon, does not desorb into the gas phase, but dissolves into the nickel, diffuses through it, and precipitates at the rear of the nickel crystallite with formation of a carbon filament.

The detailed mechanism for the formation of filamentous carbon was described in a previous paper (17) and is schematically represented for the methane cracking in Fig. 5. The model includes the following steps:

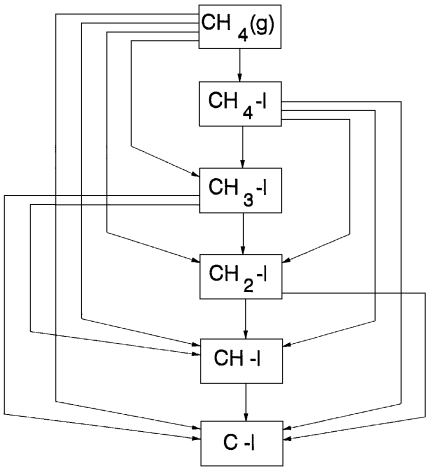

FIG. 4. Methane cracking. Possible reaction pathways.

Surface reactions:

$$\begin{aligned}
CH_4 + l &\rightleftarrows CH_4\text{-}l && K_{CH_4}\\
CH_4\text{-}l + l &\rightleftarrows CH_3\text{-}l + H\text{-}l && \text{rds}/k_M^+ \;\&\; k_M^-\\
CH_3\text{-}l + l &\rightleftarrows CH_2\text{-}l + H\text{-}l && K_3 \mid\\
CH_2\text{-}l + l &\rightleftarrows CH\text{-}l + H\text{-}l && K_4 \mid \rightarrow K_r\\
CH\text{-}l + l &\rightleftarrows C\text{-}l + H\text{-}l && K_5 \mid\\
2H\text{-}l &\rightleftarrows H_2 + 2l && 1/K_H
\end{aligned}$$

Dissolution/segregation:

$$C\text{-}l \rightleftarrows C_{Ni,f} + l \quad 1/K_C$$

Diffusion of carbon through nickel:

$$C_{Ni,f} \Rightarrow C_{Ni,r}$$

Precipitation/Dissolution of carbon:

$$C_{Ni,r} \rightleftarrows C_w \quad K_w$$

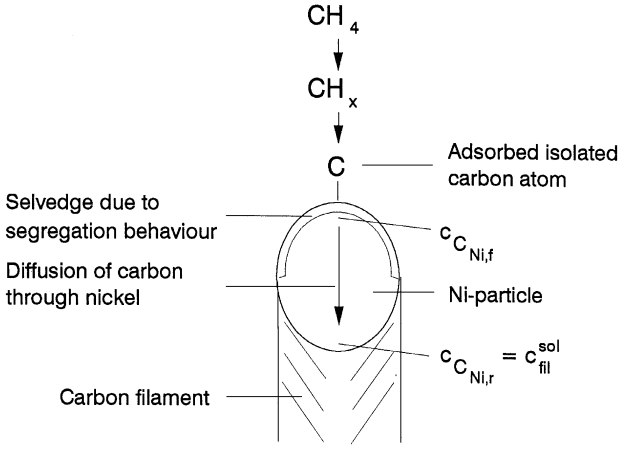

FIG. 5. Detailed mechanism of the formation of filamentous carbon by the methane cracking.

As an example, a set of surface reactions is given for a mechanism with a gradual dehydrogenation of methane and with the abstraction of the first hydrogen atom as the rate-determining step. The surface concentration of adsorbed methane and hydrogen are related to the partial pressures of methane and hydrogen by the Langmuir isotherm. The surface concentration of carbon cannot be related directly to gas-phase partial pressures. As described in the previous publication (17), it is proposed that a segregation/dissolution equilibrium exists at the gas side of the nickel particle between adsorbed carbon and carbon dissolved in nickel just below the selvedge. The segregation of carbon from the bulk nickel phase to the surface, existing of noninteracting sites, or the reverse step, the dissolution of carbon on the surface into the bulk, is described in the same way as the gas adsorption, and competition takes place between both processes:

$$C_{Ni,f} + l \rightleftarrows C\text{-}l \qquad K_c = c_{C\text{-}l}/c_{C,\{Ni,f\}} \cdot c_l.$$

Based on the Hougen–Watson approach, a rate equation can then be derived for the surface reactions. The mechanism proceeds up to carbon dissolved in nickel at the gas side of the particle, just below the selvedge ($C_{Ni,f}$, as indicated in Fig. 5). The following rate equation is derived for the mechanism in Fig. 5:

$$r_{C,M} = \frac{k_M^+ \cdot K_{CH_4} \cdot p_{CH_4} - \frac{k_M^- \cdot K_H^2 \cdot K_C}{K_3 \cdot K_4 \cdot K_5} \cdot c_{C_{Ni,f}} \cdot p_{H_2}^2}{\left(1 + K_C \cdot c_{C_{Ni,f}} + K_H^{1/2} \cdot \left(1 + \frac{K_C \cdot c_{C_{Ni,f}}}{K_5}\right) \cdot p_{H_2}^{1/2} + \frac{K_H \cdot K_C \cdot c_{C_{Ni,f}}}{K_4 \cdot K_5} \cdot p_{H_2} + \frac{K_H^{3/2} \cdot K_C \cdot c_{C_{Ni,f}}}{K_3 \cdot K_4 \cdot K_5} \cdot p_{H_2}^{3/2} + K_{CH_4} \cdot p_{CH_4}\right)^2}. \quad [2]$$

k_M^+ and k_M^- are the rate coefficients of the forward and the reverse reaction of the rate-determining step.

When the surface concentrations of H-l, CH-l and CH_2-l are negligible, the rate equation is simplified to

$$r_{C,M} = \frac{k_M^+ \cdot K_{CH_4} \cdot p_{CH_4} - \frac{k_M^{-'}}{K_r'} \cdot K_C \cdot c_{C_{Ni,f}} \cdot p_{H_2}^2}{\left(1 + K_C \cdot c_{C_{Ni,f}} + \frac{1}{K_r'} \cdot K_C \cdot c_{C_{Ni,f}} \cdot p_{H_2}^{3/2} + K_{CH_4} \cdot p_{CH_4}\right)^2}, \quad [3]$$

in which

$$k_M^{-'} = k_M^- \cdot K_H^{1/2}$$
$$K_r' = K_r/K_H^{3/2} = K_3 \cdot K_4 \cdot K_5/K_H^{3/2}.$$

The concentration of carbon dissolved in the nickel at the gas side of the particle, $c_{C,\{Ni,f\}}$, is not accessible and is eliminated by coupling the diffusion step with the rate equation for the surface reaction. The rate of diffusion of carbon through the nickel is written in terms of Fick's law:

$$r_{C,diff} = \frac{D_{C,Ni}}{d_a} \cdot (c_{C_{Ni,f}} - c_{C_{Ni,f}}) \cdot a_{Ni}. \quad [4]$$

The average diffusion path length d_a in a spherical particle with diameter d_{Ni} is $2/3 \cdot d_{Ni}$. In this description, it is assumed that all the nickel particles have the same average diameter d_{Ni}, so that the diffusion is considered to occur through a slab with thickness $2/3 \cdot d_{Ni}$, and with a surface area which is equal to the total exposed nickel surface area a_{Ni}. TEM photographs of filamentous carbon formed in methane cracking showed an average carbon filament diameter of about 16 nm.

The concentration of carbon dissolved in nickel at the support side of the particle, $c_{C,\{Ni,r\}}$, equals the saturation concentration of filamentous carbon in nickel if it is assumed that the supersaturation is very small during steady-state carbon filament growth:

$$c_{C_{Ni,r}} = c_{C_{Ni,sat}}. \quad [5]$$

At steady state, the rates of all the consecutive steps (surface reaction, dissolution, diffusion) are equal, so that $r_{C,M} = r_{C,Diff}$. The rate of diffusion is then coupled with the equation describing the rate of the surface reaction by solving it for the concentration of carbon dissolved in nickel at the gas side of the particle and inserting it into the rate equation. This leads to

$$r_{C,M} = \frac{k_M^+ \cdot K_{CH_4} \cdot p_{CH_4} - \frac{k_M^{-'}}{K_r'} \cdot K_C \cdot \left[c_{C_{Ni,sat}} + \frac{d_a}{D_{C,Ni} \cdot a_{Ni}} \cdot r_{C,M}\right] \cdot p_{H_2}^2}{\left(1 + K_C \cdot \left[c_{C_{Ni,sat}} + \frac{d_a}{D_{C,Ni} \cdot a_{Ni}} \cdot r_{C,M}\right] + \frac{1}{K_r'} \cdot K_C \cdot \left[c_{C_{Ni,sat}} + \frac{d_a}{D_{C,Ni} \cdot a_{Ni}} \cdot r_{C,M}\right] \cdot p_{H_2}^{3/2} + K_{CH_4} \cdot p_{CH_4}\right)^2}. \quad [6]$$

An implicit equation is obtained for the rate of carbon formation in methane cracking. At the coking threshold, the carbon concentration is uniform over the nickel particle ($r_{C,M} = 0$). Under conditions with an affinity for carbon formation, a certain concentration gradient develops over the nickel particle, depending on the rate coefficients and on the diffusivity $D_{C,Ni}$ (see also previous paper (17)).

Using Eq. [4], calculations were made of the concentration gradient over the nickel particle for several experimental conditions, based on literature data for the solubility and diffusivity of carbon and on the average nickel crystallite diameter determined by electron microscopy. These calculations revealed that the concentration gradient is very small for most experimental conditions (<10% of the saturation concentration). It may therefore be assumed that the concentration of carbon dissolved in nickel is almost uniform over the whole nickel particle for all experimental conditions and equal to the concentration of carbon at the support side of the particle:

$$c_{C,\{Ni,f\}} \approx c_{C,\{Ni,r\}} \approx c_{C,\{Ni,sat\}} \quad \text{since } d_a/(D_{C,Ni} \cdot a_{Ni}) \cdot r_{C,M} \ll c_{C,\{Ni,sat\}}.$$

Note that this does not imply a constant surface coverage by carbon, since the latter is determined by the competition between carbon segregation and gas adsorption, so that it also depends on the partial pressures of the gas-phase components.

Given this assumption, the term $K_c \cdot c_{C,\{Ni,sat\}}$ can be incorporated in the coefficient K_r'':

$$K_r'' = K_r'/\left(K_C \cdot c_{C,\{Ni,f\}}\right) = K_r'/\left(K_C \cdot c_{C,\{Ni,sat\}}\right).$$

If the concentration gradient were not negligibly small, the concentration of carbon dissolved in nickel at the gas side of the particle $c_{C,\{Ni,f\}}$ would vary with the conditions. In that case, an average value $c_{C,\{Ni,f\},av}$ would be incorporated into K_r''. This could lead to a poor prediction of the coking threshold, as will be discussed further.

Dividing the numerator and denominator by $(1 + K_C \cdot c_{C,\{Ni,sat\}})^2$ and incorporating this group in the other parameters leads to the following simplified form for the rate equation:

$$r_{C,M} = \frac{k_M^+ \cdot K_{CH_4} \cdot p_{CH_4} - \frac{k_M^{-'}}{K_r''} \cdot p_{H_2}^2}{\left(1 + \frac{1}{K_r''} \cdot p_{H_2}^{3/2} + K_{CH_4} \cdot p_{CH_4}\right)^2}. \qquad [7]$$

This type of kinetic equation will be called further the nonreversible model description, since it is described by a forward and a reverse rate coefficient, without incorporation of the experimentally determined threshold constant. The parameters of Eq. [7] were estimated by simultaneous regression of all experiments at all temperatures.

The incorporation of the term $(1 + K_C \cdot c_{C,\{Ni,sat\}})$ in the other parameters could influence the Arrhenius dependence of these parameters. This influence is negligible if the surface carbon coverage is very small or if this term shows only a small temperature dependence. A small temperature dependence would not be surprising since the solubility increases with the temperature, while K_C, the segregation equilibrium constant, decreases with the temperature, and since the heat of precipitation and the heat of segregation are almost equal, according to Isett *et al.* (25).

Kinetic determination of the coking threshold. In the following, it is checked if the model correctly predicts the coking threshold. Referring to the rate Eq. [6], which incorporates the diffusion step, it is seen that there is a uniform carbon concentration over the nickel particle at the coking threshold ($r_{C,M} = 0$; $c_{C,\{Ni,f\}} = c_{C,\{Ni,sat\}}$). By equating the rate of carbon formation to zero, an expression can be derived for the kinetic threshold constant, which is the ratio of the lumped rate coefficients for the forward and the reverse reaction of the rate-determining step:

$$\left(\frac{p_{H_2}^2}{p_{CH_4}}\right)_{r_{C,M}=0} = \frac{k_M^+ \cdot K_{CH_4}}{\frac{k_M^{-'}}{K_r'} \cdot K_C \cdot c_{C,\{Ni,sat\}}} = \frac{k_M^{+''}}{k_M^{-''}} = K_M^{kin} = K_M^*. \qquad [8]$$

Incorporation of the diffusion step into the rate equation permits to account for the varying concentration $c_{C,\{Ni,f\}}$ at the gas side of the nickel particle, so that the kinetic threshold constant will equal the experimentally determined threshold constant. For the parameter estimation, the term $K_C \cdot c_{C,\{Ni,f\}}$ was incorporated into the coefficient K_r'' under the assumption that the carbon concentration in nickel is almost uniform for all experimental conditions: $c_{C,\{Ni,f\}} = c_{C,\{Ni,sat\}}$. If this assumption is valid, the ratio of the lumped rate coefficients obtained from the parameter estimation will equal the experimentally observed threshold constant and the rate equation will predict the coking threshold correctly. If the concentration gradients are nonnegligible, some average value $c_{C,\{Ni,f\},av}$, higher than $c_{C,\{Ni,sat\}}$, enters into the rate coefficient $k_M^{-''}$:

$$\left(\frac{p_{H_2}^2}{p_{CH_4}}\right)_{r_{C,M}=0} = \frac{k_M^+ \cdot K_{CH_4}}{\frac{k_M^{-'}}{K_r'} \cdot K_C \cdot c_{C_{Ni,f,av}}} = \frac{k_M^{+''}}{k_M^{-''}} = K_M^{kin} < K_M^*. \qquad [9]$$

In this case, the ratio of the lumped rate coefficients does not correspond to the coking threshold.

Approximate reversible description of the methane cracking. Until now, the rate equations were described in the nonreversible way, with a forward and a reverse rate coefficient for the rate-determining step. Since the rate-determining step is a reversible elementary surface reaction, these rate coefficients are linked by the equilibrium constant for this particular reaction step. In a heterogeneously catalyzed reaction with formation of only gaseous reaction products, the ratio of the lumped rate coefficients for the forward and the reverse reaction of the rate-determining step equals the equilibrium constant for the global reaction. The global equilibrium constant is the product of the equilibrium constants of all the elementary

steps in the reaction mechanism and may be inserted into the rate equation. In the case considered here, one of the reaction products is a solid, namely filamentous carbon. The experimentally derived threshold constant, which is determined by the thermodynamic properties of filamentous carbon, separates the regions where there is a positive or a negative net rate of carbon formation. The way in which it can be entered into the rate equation is not as straightforward as the introduction of the equilibrium constant into the rate equation for a heterogeneously catalyzed reaction with only gaseous reaction products, since the carbon filament formation also involves a diffusion step. The diffusion cannot be treated as a normal elementary surface reaction step: the diffusion is a nonreversible process and operates in one direction only.

The rate Eq. [6] for the nonreversible description of the methane cracking can be written

$$r_{C,M} = \frac{k_M^+ \cdot K_{CH_4} \cdot \left(p_{CH_4} - \frac{k_M^{-'} \cdot K_C \cdot c_{C_{Ni,f}}}{K_r' \cdot k_M^+ \cdot K_{CH_4}} \cdot p_{H_2}^2\right)}{\left(1 + K_C \cdot c_{C_{Ni,f}} + \frac{1}{K_r'} \cdot K_C \cdot c_{C_{Ni,f}} \cdot p_{H_2}^{3/2} + K_{CH_4} \cdot p_{CH_4}\right)^2}. \quad [10]$$

For high values of the diffusivity, the concentration of carbon dissolved in nickel is almost uniform ($c_{C,\{Ni,f\}} \approx c_{C,\{Ni,sat\}}$), and the rate equation finally becomes, accounting for Eq. [8],

$$r_{C,M} = \frac{k_M^+ \cdot K_{CH_4} \cdot \left(p_{CH_4} - \frac{1}{K_M^*} \cdot p_{H_2}^2\right)}{\left(1 + \frac{1}{K_r''} \cdot p_{H_2}^{3/2} + K_{CH_4} \cdot p_{CH_4}\right)^2}. \quad [11]$$

This is the model based on the experimentally observed threshold constant and which is forced to predict the coking threshold correctly. This rate equation is correct only at the coking threshold, where the concentration in the nickel particle is completely uniform ($c_{C,\{Ni,f\}} = c_{C,\{Ni,r\}} = c_{C,\{Ni,sat\}}$). At the coking threshold itself, the diffusion step is eliminated from the global reaction mechanism. This description is also justified if the diffusivity is sufficiently high and the concentration gradients small. Equation [11] corresponds with an *"approximate" reversible* model.

Model discrimination. In the same way and under the same assumptions, rate equations were derived for all the possible pathways and rate-determining steps, yielding a total of 80 different rate equations. These rate equations can be categorized into families of models, each having a certain driving force term (numerator). With the exception of the first family, a certain rate-determining step gives rise to a specific driving force term. Therefore, these families are also families of models with the same rate determining step. They are presented in Table 1. For a mechanism with a gradual abstraction of hydrogen atoms and with, respectively, a molecular and a dissociative adsorption of methane, the corresponding denominator is also shown in Table 1.

TABLE 1

Categorization into Families of Models with the Same Driving Force Term and the Same Rate-Determining Step

Driving force I	$k_M^{+''} \cdot p_{CH_4} - k_M^{-''} \cdot p_{H_2}^2$
Rate-determining step	Adsorption of CH_4 or reaction of CH_4-l
Denominator^{ma}	$(1 + K_1'\sqrt{p_{H_2}} + K_2' p_{H_2} + K_3' p_{H_2}^{3/2} + K_4' p_{CH_4})^2$
Denominator^{da}	$(1 + K_1'\sqrt{p_{H_2}} + K_2' p_{H_2} + K_3' p_{H_2}^{3/2})^2$
Driving Force II	$k_M^{+''} \cdot \frac{p_{CH_4}}{p_{H_2}^{1/2}} - k_M^{-''} \cdot p_{H_2}^{3/2}$
Rate-determining step	Reaction of CH_3-l
Driving Force III	$k_M^{+''} \cdot \frac{p_{CH_4}}{p_{H_2}} - k_M^{-''} \cdot p_{H_2}$
Rate-determining step	Reaction of CH_2-l
Driving Force IV	$k_M^{+''} \cdot \frac{p_{CH_4}}{p_{H_2}^{3/2}} - k_M^{-''} \cdot p_{H_2}^{1/2}$
Rate-determining step	Reaction of CH-l
Driving Force V	$k_M^{+''} \cdot p_{CH_4}^{1/2} - k_M^{-''} \cdot p_{H_2}$
Rate-determining step	H_2 desorption

Note. For driving force I, the denominator of the rate equation is also presented for a model with a gradual abstraction of hydrogen atoms and, respectively, with a molecular (^{ma}) and a dissociative (^{da}) adsorption of methane.

A number of criteria were used in the model discrimination. The first step in the model discrimination was the inspection of the behavior of the models with respect to the influence of the partial pressures of hydrogen and methane. It was experimentally observed that the rate of carbon formation does not show a monotonous increase with the partial pressure of methane for a constant partial pressure of hydrogen, but starts to decrease from certain values onward. The models in which a dissociative adsorption of methane is proposed, or the models with the adsorption of methane as the rate-determining step, were rejected on this basis, since they do not contain a term related to the partial pressure of methane in the denominator (Table 1). A number of models predict a zero rate of carbon formation at $p_{H_2} = 0$ bar. It became clear from the experiments that the rate does not tend to zero at $p_{H_2} = 0$. The strong decrease for $p_{CH_4} = 1.5$ bar is due to deactivation and does not originate from a rate of the methane cracking tending to zero.

The second step in the model discrimination was based on the parameter estimation and the fit for one temperature. The resultant parameter estimates were subjected to a statistical analysis. It was checked if the model fits well (F test and adequacy test) and if the parameters are significantly positive (t test).

The t test is used to verify if the estimate differs from zero:

$$t_c = \frac{|b_j|}{s(b_j)} > t_{tab}(n - p; 97.5\%).$$

The F value for the F test is defined as

$$F_c = \frac{(\text{regression sum of squares}/p)}{(\text{residual sum of squares}/n-p)} = \frac{\sum_{i=1}^{n} \frac{\hat{y}_i^2}{p}}{\sum_{i=1}^{n} \frac{(y_i-\hat{y}_i)^2}{(n-p)}} > F_{\text{tab}}(p, n-p; 95\%).$$

The higher the F value, the better the model.

For the adequacy test, another F value is defined

$$F_c = \frac{(\text{lack of fit sum of squares}/n-p-n_e+1)}{(\text{pure error sum of squares}/n_e-1)} = \frac{\frac{\sum_{i=1}^{n}(y_i-\hat{y}_i)^2-\sum_{j=1}^{n_e}(y_j-\bar{y}_j)^2}{(n-p-n_e+1)}}{\sum_{j=1}^{n_e}\frac{(y_j-\bar{y}_j)^2}{(n_e-1)}} < F_{\text{tab}}(n-p-n_e+1, n_e-1; 95\%).$$

The pure error sum of squares is calculated from replicate experiments. This F value is compared with the tabulated 95 percentage point of the F distribution with $n-p-n_e+1$ and n_e-1 degrees of freedom. If the calculated value exceeds the tabulated value, the model can be rejected because of a lack of fit. More details of the procedure are provided by Froment and Bischoff (18) and Froment and Hosten (19).

The parameters should also satisfy certain physicochemical constraints. The most important constraints are that the parameter estimates should be positive, that rate coefficients should increase and adsorption coefficients decrease with the temperature.

Only one of the 80 possible rate equations satisfied all these criteria. This rate equation corresponds to a mechanism with a gradual dehydrogenation of adsorbed methane and with the abstraction of the first hydrogen atom and the formation of a methyl group as the rate-determining step (Fig. 5). The rate Eqs. [7] and [11] given above correspond to this mechanism.

The results of the parameter estimation are presented in Table 2. All the parameters are significantly different from zero, except the heat of adsorption of methane. An excellent fit is seen ($F=1972$), and the model cannot be rejected because of a lack of fit, since the calculated value is smaller than the tabulated one. The comparison of the experimental rates of carbon formation at 500°C, obtained in the sequential experiments on used catalysts, and the model predictions is presented in Fig. 6, while the parity diagram for experiments between 500 and 550°C is given in Fig. 7. The prediction is excellent, also at high partial pressures of hydrogen, near the coking threshold. The prediction of the rate of carbon formation near the threshold is less accurate at low partial pressures of methane. This is due to the different value for the threshold constant at $p_{CH_4}=1.5$ bar and $p_{CH_4}=10$ bar. The agreement between the ratio of the lumped rate coefficients and the experimentally determined threshold constant is shown in Table 3.

TABLE 2

Nonreversible Model Description

		Estimate	t value	Lower limit	Upper limit
k_M^+	A_M^+ (mol/gcat h)	23444	31.8[a]	3.07[a]	3.48[a]
	E_M^+ (J/mol)	59033	6.9	41950	76120
$k_M^{-'}$	$A_M^{-'}$ (mol/gcat bar$^{1/2}$ h)	4389	13.4[a]	0.42[a]	0.56[a]
	$E_M^{-'}$ (J/mol)	60522	3.2	22460	98580
K_{CH_4}	A_{CH_4} (bar^{-1})	0.21	26.5[a]	0.19[a]	0.23[a]
	$\Delta H^0_{CH_4}$ (J/mol)	143	0.1	−20440	20730
K_r''	A_r'' (bar$^{3/2}$)	1.109×10^8	23.0[a]	0.11[a]	0.13[a]
	$\Delta H_r^{0''}$ (J/mol)	137314	11.9	114200	160400

F value	1972
Residual SSQ	0.0231 ($n-p=52$)
Pure error SSQ	0.0023 ($n_e-1=6$)
Lack of fit SSQ	0.021 ($n-p-n_e+1=46$)
F_C	$1.159 < F_{\text{tab}}$ (46, 6; 95%) = 3.76

Note. Parameter estimates based on the simultaneous regression of all experiments at all temperatures, t values, and approximate 95% confidence intervals; F value; and adequacy test for the selected model, based on experiments sequentially performed on "used" catalyst samples.

[a] Based on reparameterized coefficients.

Parameters were also estimated for the "approximate" reversible model. The value for K_M^* at $p_{CH_4}=5.0$ bar was used. The results of the parameter estimation are presented in Table 4. The agreement between the nonreversible and the reversible model is excellent. This is logical since the ratio of the forward and reverse rate coefficients was

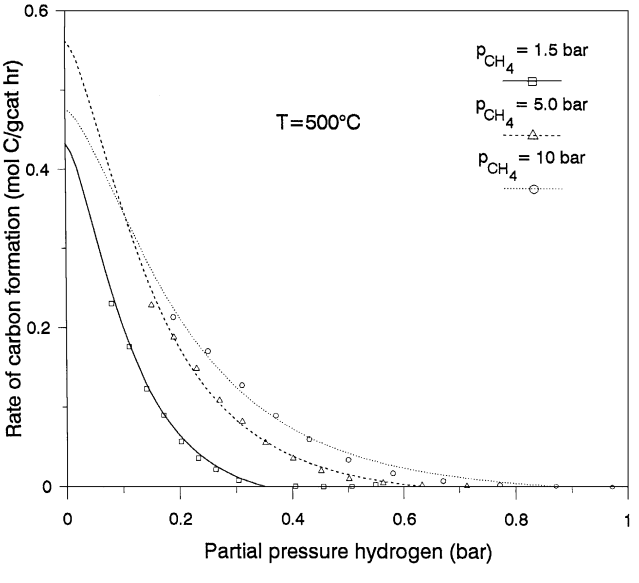

FIG. 6. Methane cracking: experimental results for the sequential experiments on "used" catalyst samples and model predictions. $T=500$°C.

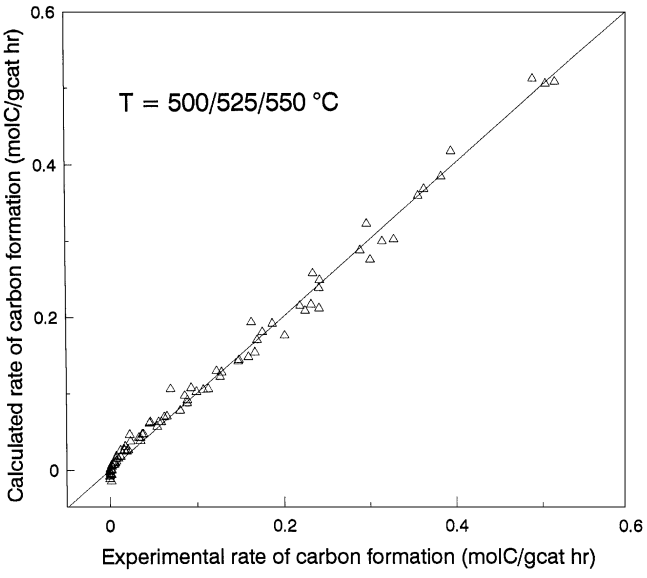

FIG. 7. Methane cracking: Parity diagram based on the results for the sequential experiments on used catalyst samples.

already found to be close to the experimental threshold constant.

DISCUSSION

Comparison with Literature Data

The kinetic model that has been derived on the basis of the parameter estimation and model discrimination proposes a gradual dehydrogenation of methane, with the abstraction of the first hydrogen atom from molecularly adsorbed methane as the rate-determining step. This mechanism corresponds well with the mechanisms that are proposed on the basis of molecular beam studies (5–9) and kinetic studies (14–16) of the methane cracking, except for the adsorption step of methane. According to these studies (5–16), methane adsorbs dissociatively by a direct process, whereas the model presented here assumes that adsorbed methane acts as an intermediate. This difference could arise

TABLE 3

Comparison of the Ratio of the Lumped Rate Coefficients of the Forward and Reverse Reaction of the Rate-Determining Step and the Experimentally Determined Threshold Constant

T (°C)	$k_M^{+\prime\prime}/k_M^{-\prime\prime}$	$K_M^*(p_{CH_4} = 10$ bar)
500	0.08	0.11
525	0.16	0.20
550	0.30	0.40

Note. Kinetic modeling based on the experiments sequentially performed on "used" catalyst samples.

TABLE 4

Approximate Reversible Model Description

		Estimate	t value	Lower limit	Upper limit
k_M^+	A_M^+ (mol/gcat h)	25040	26.1[a]	3.30[a]	3.85[a]
	E_M^+ (J/mol)	58893	5.5	37670	80120
K_{CH_4}	A_{CH_4} (bar^{-1})	0.21	21.0[a]	0.18[a]	0.21[a]
	$\Delta H^0_{CH_4}$ (J/mol)	567	0.04	−25500	26640
K_r''	A_r'' (bar$^{3/2}$)	5.18×10^7	22.4[a]	0.09[a]	0.11[a]
	$\Delta H_r^{0\prime\prime}$ (J/mol)	133210	10.9	108800	157600
F value		1754			

Note. Parameter estimates based on the simultaneous regression of all experiments at all temperatures, t values, and approximate 95% confidence limits, and F value for the selected model, based on experiments sequentially performed on "used" catalyst samples.

[a] Based on reparameterized coefficients.

from the fact that the molecular beam studies and the studies in which AES is used to follow the rate of carbon buildup are performed in a completely different pressure range. The kinetic studies performed by Alstrup *et al.* (14, 15) are also performed at partial pressures of methane lower than 1 atm. As became clear from the experiments reported here, the decrease of the rate of the methane cracking with the partial pressure of methane, pointing toward the presence of molecularly adsorbed methane, is observed only at very high pressure ($p_{CH_4} > 5$ bar). Another important difference between Alstrup *et al.* (14, 15) and this work is the description of the carbon filament formation. Alstrup assumed that the carbon surface coverage has a fixed value, independent of the operating conditions so that abstraction is made of the subsequent steps in the carbon filament formation. In the model proposed here it is assumed that the carbon coverage is determined by the competition between carbon segregation and gas adsorption, two similar processes. Evidence for this description was given in a previous publication (17) and was mainly based on studies presented in the literature on carbon segregation and on results for the gasification of filamentous carbon by hydrogen. The assumption that was made in the present work, namely an almost uniform concentration of carbon dissolved in nickel due to a sufficiently high diffusivity $D_{C,Ni}$, does not modify this behavior.

The rate-determining step, the abstraction of the first hydrogen atom, corresponds well with the results in the literature. From studies with the molecular beam technique, a threshold energy necessary to overcome the energy barrier of 52 kJ/mol was found, close to the value of 59 kJ/mol determined in this work. From studies in which the rate of carbon deposition was followed by AES, an apparent activation energy of 27–56 kJ/mol was obtained, depending on the Ni surface that was studied (10, 12). Chorkendorf *et al.* (26) used XPS to monitor the amount of carbon deposited on the surface. They studied the interaction of methane with

TABLE 5

Chemisorption Energies of CH_x Species and H on Ni(100)

Adsorbate	Chemisorption energy (kJ/mol)
C	627[a]
CH	568[a]
CH_2	380[a]
CH_3	192[a]
H	263[b]

[a] Siegbahn *et al.* (29).
[b] Christmann *et al.* (31).

the Ni(100) surface between 400 and 550 K at a methane pressure of 1 Torr, and determined an apparent activation energy for the initial sticking coefficient of 52 kJ/mol. Theoretical studies were published on the chemisorption of methane on various nickel surfaces (27, 28). Yang *et al.* (28) calculated an activation energy of 70 kJ/mol. According to Alstrup *et al.* (14, 15), both the dissociative adsorption of methane with formation of an adsorbed methyl group and the dehydrogenation of the adsorbed methyl group deviate from equilibrium. Their data at different temperatures (15) indicate that it is more probable that the dissociative adsorption step, with formation of the adsorbed methyl group, is the rate-determining step.

The results of the present work can also be compared with the results of cluster model calculations, performed by Siegbahn *et al.* (27) for CH_x species chemisorbed on Ni(100) and Ni(111), listed in Table 5. These values can be combined with the bond dissociation enthalpies for methane and hydrogen, mentioned in Table 6, to calculate the enthalpy change corresponding with each elementary surface reaction step. From these values, an energy scheme can be constructed for methane cracking, shown in Fig. 8. Not all the enthalpy changes of the elementary steps could be estimated from the kinetic study. The reaction mechanism and the energy scheme, based on the cluster model calculations, were simplified in the same way as for the parameter estimation, to allow a clear cut comparison. The activation energy

TABLE 6

Bond Dissociation Enthalpies for Methane and Hydrogen

CH_4
- Mean bond dissociation enthalpy, 415 kJ/mol
- Bond dissociation enthalpies
  - H–C, 339 kJ/mol
  - H–CH, 426 kJ/mol
  - $H–CH_2$, 459 kJ/mol
  - $H–CH_3$, 435 kJ/mol

H_2
- Bond dissociation enthalpy, 436 kJ/mol

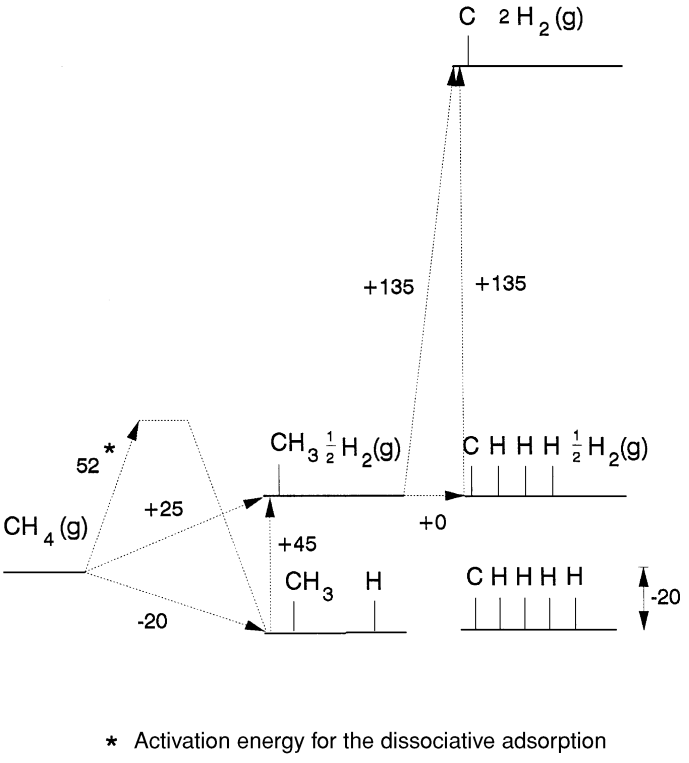

FIG. 8. Energy scheme for the methane cracking based on cluster model calculations on Ni(100) by Siegbahn *et al.* (29).

that is given for the dissociative adsorption in Fig. 8 is a typical literature value. The energy diagram derived from the present study is shown in Fig. 9. The activation energies for the rate-determining step are also given. Since the heat of segregation and the heat of precipitation of carbon are more or less equal (10 kcal/mol (25)), the temperature dependence for the term $K_C \cdot c_{C,\{Ni,sat\}}$ is very weak, so that the enthalpy change for the formation of adsorbed carbon atoms and whisker carbon is more or less equal. The adsorption coefficient K_H could not be estimated, since it was not significantly different from zero in the parameter estimation. A literature value for the heat of adsorption was used to calculate ΔH_r^0 and E_M^-. Christmann (29) determined a heat of adsorption of hydrogen on Ni(100) of 92 kJ/mol. Using TPD Konvalinka *et al.* (30) identified a number of adsorbed states of hydrogen on Ni catalysts. An average value for the heat of adsorption of about 72 kJ/mol can be calculated from their results. Bartholomew *et al.* (31) give an overview of the studies on the adsorption of hydrogen on nickel. An average value for the heat of adsorption of H_2 on polycrystalline Ni of 80 kJ/mol was used for the energy diagram. Both energy schemes compared very well, which is further support for the validity of the selected model and the corresponding mechanism. Note that the surface dehydrogenation is slightly exothermic and that the global reaction becomes endothermic by the desorption of hydrogen.

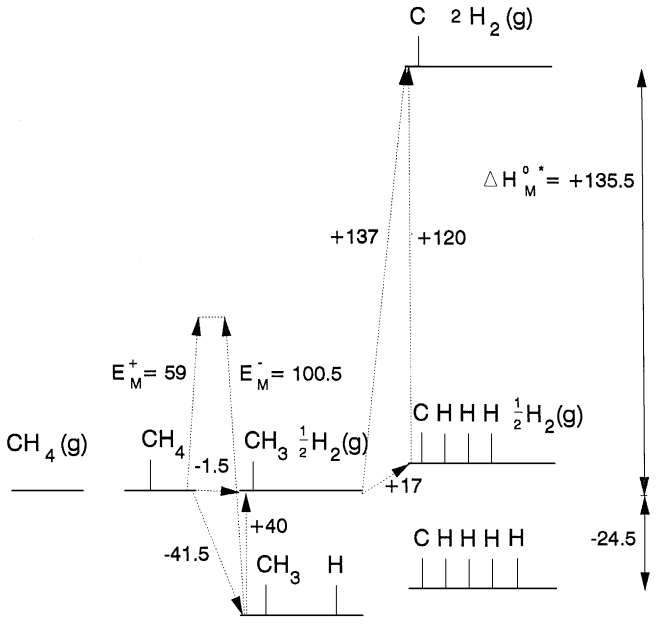

FIG. 9. Energy scheme for the methane cracking derived from the present work.

Nucleation and Deactivation of Filamentous Carbon Growth Described by the Model for the Methane Cracking with Incorporation of the Diffusion Step

The mechanism that is selected here for the methane cracking, described by rate Eq. [7], shows an excellent prediction of the experimentally observed rates of carbon formation. It may be concluded that the assumption of a more or less uniform concentration of carbon in nickel due to a sufficiently high diffusivity of carbon in nickel is acceptable.

The use of rate Eq. [6] without simplifications, allows to collect interesting qualitative information concerning the nucleation and deactivation of filamentous carbon growth. As has been mentioned in paragraph 2, encapsulating carbon was formed in the absence of hydrogen at low partial pressures of methane ($p_{CH_4} = 1.5$ bar), causing a rapid deactivation of the catalyst. No deactivation was observed at high partial pressures of methane ($p_{CH_4} = 5.0$ bar and 10.0 bar). The different behavior can be explained in terms of the fractional carbon surface coverage:

$$\theta_C = \frac{K_C \cdot c_{C_{Ni,f}}}{1 + K_C \cdot c_{C_{Ni,f}} + \frac{K_C}{K_r'} \cdot c_{C_{Ni,f}} \cdot p_{H_2}^{3/2} + K_{CH_4} \cdot p_{CH_4}}. \quad [12]$$

It is clear that the carbon surface coverage in the absence of hydrogen will be much higher at low partial pressures of methane, so that attractive interactions and C–C bonds become more likely, explaining the occurrence of deactivation at low partial pressure of methane in the absence of hydrogen. This behavior results from the competition between carbon segregation and gas adsorption for the same adsorption sites. The presence of attractive interactions among adsorbed carbon atoms at higher coverages was also deduced from carbon segregation studies (25, 32).

During the nucleation of carbon filaments, there is no carbon deposition yet and the rates of all the consecutive steps are zero, although there is a clear affinity for carbon formation. As described in the previous paper (17), a certain supersaturation of carbon in nickel with respect to filamentous carbon is present, depending upon the affinity of the gas mixture for carbon formation. Because of the segregation equilibrium, this results also in a high carbon surface concentration, so that the net rate of carbon formation is zero. The uniform concentration of carbon dissolved in nickel during the nucleation can be calculated by equating the rate of carbon formation (6) to zero, and solving for $c_{C,\{Ni,nucl\}}$:

$$\Rightarrow c_{C_{Ni,nucl}} = \frac{k_M^+ \cdot K_{CH_4} \cdot K_r'}{k_M^{-'} \cdot K_C} \cdot \frac{p_{CH_4}}{p_{H_2}^2} \quad [13]$$

or, accounting for Eq. [8]

$$c_{C_{Ni,nucl}} = K_M^* \cdot c_{C_{Ni,sat}} \cdot \frac{p_{CH_4}}{p_{H_2}^2} \quad [14]$$

The expression for the concentration of carbon dissolved in nickel during the nucleation (14) shows that this concentration increases with the affinity for methane cracking, i.e., for high partial pressure of methane, low partial pressure of hydrogen, or high temperature (high value for K_M^*). Since it is logical to suppose that the nucleation is easier as the carbon concentration exceeds more the saturation concentration of filamentous carbon, it can be expected that the nucleation is easier if conditions with a higher affinity for carbon formation are applied. This confirms the observations regarding the nucleation of filamentous carbon that were reported in the previous publication (17). Due to the high surface converage of carbon during nucleation, it can also be expected that the risk for deactivation is largest during carbon filament nucleation. Once the growth has started, both the concentration of carbon dissolved in nickel and the surface coverage of carbon decrease.

The expression derived for $c_{C,\{Ni,nucl\}}$ is valid for all cases in which a gas mixture is sent over a catalyst sample on which no carbon filaments are present yet. If the mixture shows an affinity for carbon formation ($p_{H_2}^2/p_{CH_4} < K_M^*$), nucleation of carbon filaments will take place, since $c_{C,\{Ni,nucl\}} > c_{C,\{Ni,sat\}}$. If the mixture shows an affinity for gasification ($p_{H_2}^2/p_{CH_4} > K_M^*$), there will be no nucleation of carbon filaments since $c_{C,\{Ni,nucl\}} < c_{C,\{Ni,sat\}}$. In that case, a low uniform concentration of carbon in Ni is obtained, depending on the composition of the mixture.

CONCLUSIONS

A kinetic modeling of the formation of filamentous carbon by the methane cracking was performed based on an experimental study in an electrobalance setup under realistic partial pressures of methane and hydrogen. Series of experiments were sequentially performed on "used" catalyst samples, on which carbon was first deposited under standard conditions with a high affinity for carbon formation, so that the experimentally observed rates of carbon formation are all based on the same number of growing carbon filaments.

The kinetic model was based on a detailed description of the carbon filament formation. The kinetic modeling led to two types of equations: the nonreversible version in which the rate-determining step contains forward and reverse contributions and the approximate reversible version, in which the experimentally determined threshold constant is introduced. The nonreversible model only predicts the coking threshold correctly if the assumption of a negligibly small concentration gradient is valid. The reversible model is only rigorously valid at the coking threshold, where the carbon concentration in nickel is uniform, or also approximately valid further away from the threshold, if the concentration gradients are negligibly small.

A mechanism is arrived at for the methane cracking which consists of a gradual dehydrogenation of molecularly adsorbed methane. The rate-determining step is the abstraction of the first hydrogen atom from molecularly adsorbed methane with the formation of an adsorbed methyl group. An excellent agreement with the experimental data is obtained. The model equation separates correctly the two regions where there exists, respectively, an affinity for carbon formation and gasification. The boundaries of the region were determined experimentally and are reflected in the threshold constant. It also appears that the assumption of an almost uniform carbon concentration is acceptable: the presence of significant concentration gradients for certain conditions would result in a poor prediction of the coking threshold.

The energy diagram for the methane cracking based on the results of the parameter estimation corresponds well with the one based on literature data, except for the adsorption step of methane that is generally considered as dissociative.

The rigorous kinetic modeling with incorporation of the diffusion step allows to explain the deactivation of carbon filament growth and the influence of the affinity for carbon formation on the nucleation of filamentous carbon.

APPENDIX: NOMENCLATURE

a_{Ni}	Nickel metal surface area [m^2/g_{cat}]
b_j	Parameter estimate
$c_{Ni,f}$	Carbon dissolved in nickel at the front of the particle, just below the selvedge
$c_{C,\{Ni,f\}}$	Concentration of carbon dissolved in nickel at the front of the particle, just below the selvedge (gas side) ($molC/m^3_{Ni}$)
$c_{C,\{Ni,r\}}$	Concentration of carbon dissolved in nickel at the rear of the particle (support side) ($molC/m^3_{Ni}$)
$c_{C,\{Ni,sat\}}$	Saturation concentration of filamentous carbon in nickel ($molC/m^3_{Ni}$)
$c_{C,\{Ni,nucl\}}$	Concentration of carbon in nickel during carbon filament nucleation ($molC/m^3_{Ni}$)
c_{C-l}	Surface carbon concentration
d_a	Average diffusion path length (m)
d_{Ni}	Average nickel crystallite diameter (m)
$D_{C,Ni}$	Diffusivity of carbon in nickel (m^2/h)
K^*_M	Experimentally determined threshold constant for the methane cracking
K^{kin}_M	Kinetic threshold constant for the methane cracking, equal to the ratio of the lumped rate coefficients for the forward and the reverse reaction of the rate-determining step
K^{gr}_M	Equilibrium constant for the methane cracking with formation of graphite
$K^{Ni_3C}_M$	Equilibrium constant for the methane cracking with formation of nickel carbide
K	Symbol used for equilibrium coefficients
k^+_M, k^-_M	Rate coefficients of the forward and the reverse reaction of the rate-determining step
l	Empty catalyst site
n	Number of experiments
n_e	Number of replicate observations
p	Number of parameters
p_i	Partial pressure of component i
$r_{C,M}$	Rate of carbon filament formation by the methane cracking (molC/gcat h)
$r_{C,diff}$	Rate of carbon diffusion through nickel (molC/gcat h)
$s(b_j)$	Unbiased estimate for the standard deviation
y_i	Experimental observation of dependent variable y
$\hat{y}_i$	Calculated value of the dependent variable y
$\bar{y}_i$	Arithmetic mean of n_e replicate observations
$\mu_{C,fil}$	Chemical potential of filamentous carbon

ACKNOWLEDGMENTS

The authors are grateful to ICI Chemicals and Polymers Ltd., Billingham, UK, for funding this research project.

REFERENCES

1. Trimm, D. L., *Catal. Rev.-Sci. Eng.* **16**, 155 (1977).
2. Bartholomew, C. H., *Catal. Rev.-Sci. Eng.* **24**, 67 (1982).

3. Rostrup-Nielsen, J. R., Catalytic steam reforming, *in* "Catalysis, Science and Technology," Vol. 5, p. 1. Springer, Berlin, 1984.
4. Deleted in proof.
5. Lee, M. B., Yang, Q. Y., Tang, S. L., and Ceyer, S. T., *J. Chem. Phys.* **85**, 1693 (1986).
6. Lee, M. B., Yang, Q. Y., and Ceyer, S. T., *J. Chem. Phys.* **87**, 2724 (1987).
7. Beckerle, J. D., Yang, Q. Y., Johnson, A. D., and Ceyer, S. T., *J. Chem. Phys.* **86**, 7236 (1987).
8. Ceyer, S. T., Beckerle, J. D., Lee, M. B., Tang, S. L., Tang, Q. Y., and Hines, M. A., *J. Vac. Sci. Technol.* **A5**, 501 (1987).
9. Hamza, A. V., and Madix, R. J., *Surf. Sci.* **179**, 25 (1987).
10. Beebe, T. P., Goodman, D. W., Kay, B. D., and Yates, T. Y., *J. Chem. Phys.* **87**, 2305 (1987).
11. Sault, A. G., and Goodman, D. W., *J. Chem. Phys.* **88**, 7232 (1988).
12. Jiang, X., and Goodman, D. W., *Catal. Lett.* **4**, 173 (1990).
13. Hanley, L., Xu, Z., and Yates, J. T., *Surf. Sci. Lett.* **248**, L265 (1991).
14. Alstrup, I., and Tavares, M. T., *J. Catal.* **135**, 147 (1992).
15. Alstrup, I., and Tavares, M. T., *J. Catal.* **139**, 513 (1993).
16. Demicheli, M. C., Ponzi, E. N., Feretti, O. A., and Yeramian, A. A., *Chem. Eng. J.* **46**, 129 (1991).
17. Snoeck, J.-W., Froment, G. F., and Fowles, M., *J. Catal.* **169**, 240 (1997).
18. Froment, G. F., and Bischoff, K. B., "Chemical Reactor Analysis and Design." Wiley, New York, 1990.
19. Froment, G. F., and Hosten, L., "Catalytic Kinetics: Modeling." Catalysis Science and Technology, 1981.
20. Rostrup-Nielsen, J. R., *J. Catal.* **27**, 343 (1972).
21. Manning, M. P., Garmirian, J. E., and Reid, R. C., *Ind. Eng. Chem. Process Des. Dev.* **21**, 404 (1982).
22. De Bokx, P. K., Kock, A. J. H. M., Boellaard, E., Klop, W., and Geus, J. W., *J. Catal.* **96**, 454 (1985).
23. Alstrup, I., *J. Catal.* **109**, 241 (1988).
24. Takeuchi, A., and Wise, H., *J. Phys. Chem.* **87**, 5372 (1983).
25. Isett, L. C., and Blakely, J. M., *Surf. Sci.* **58**, 397 (1976).
26. Chorkendorff, I., Alstrup, I., and Ullmann, S., *Surf. Sci.* **227**, 291 (1990).
27. Siegbahn, P. E. M., and Panas, I., *Surf. Sci.* **240**, 37 (1990).
28. Yang, H. Y., and Whitten, J. L., *J. Chem. Phys.* **96**, 5529 (1992).
29. Christmann, K., *Z. Naturforsch.* **34a**, 22 (1979).
30. Konvalinka, J. A., Oeffelt, P. H., and Scholten, J. J. F., *Appl. Catal.* **1**, 141 (1981).
31. Bartholomew, C. H., *Catal. Lett.* **7**, 27 (1990).
32. Vajo, J. J., and McCarty, J. G., *Appl. Surf. Sci.* **47**, 23 (1991).